

Tailored Phase Transitions via Mixed-Mesogen Liquid Crystalline Polymers with Silicon-Based Spacers

Ingrid A. Rousseau,^{†,‡} Haihu Qin,^{†,§} and Patrick T. Mather^{*,†,||}

Institute of Materials Science and Chemical Engineering Department, University of Connecticut, Storrs, Connecticut 06269

Received August 13, 2004; Revised Manuscript Received February 22, 2005

ABSTRACT: Control over thermotropic phase behavior in low- T_g main-chain liquid crystalline polymers (LCPs) is desired for a variety of applications, including soft actuation when cross-linked. Here, we describe the synthesis of new silicon-based main-chain LCPs, including homopolymers, blends, and copolymers, with tunable clearing temperatures as governed by their chemical composition. Two mesogenic groups, namely, 1,4-bis[4-(4-pentenyl)oxy]benzoyl]hydroquinone (\mathbf{M}_1) and 2-*tert*-butyl-1,4-bis[4-(4-pentenyl)oxy]benzoyl]hydroquinone (\mathbf{M}_2), were polymerized with various silicon-based flexible spacers, specifically, 1,4-bis(dimethylsilyl)benzene (\mathbf{S}_1), 1,1,3,3,5,5-hexamethyltrisiloxane (\mathbf{S}_2), and hydride-terminated poly(dimethylsiloxane) (DP = 8) (\mathbf{S}_3) spacers, following routine hydrosilation reaction techniques. These mesogens and flexible spacers were chosen so that both copolymerization and blending of homopolymers would allow for potential tailoring of phase behavior. Indeed, despite their similar chemical structure, the clearing transition temperatures of \mathbf{M}_1 and \mathbf{M}_2 differ dramatically ($\Delta T_{NI} = 140$ °C), while the silicon-based spacers offer accessibility to a large range of molecular flexibility. High-molecular-weight LCPs were successfully prepared using Pt-catalyzed addition polymerization. Interestingly, the polymers exhibited wide liquid crystalline windows with relatively high degree of order (smectic phases) except for the \mathbf{S}_1 -based blends, which, in addition to a smectic phase, also displayed a narrow nematic phase. As expected, a drastic decrease of the glass transition temperature arose on polymerizing with longer, more flexible spacers, from about 56 to -17 °C. Finally, in comparing the two approaches to phase behavior tailoring, namely, blending vs copolymerization, the former led to apparently immiscible systems with constant isotropization temperatures, while the latter yielded homogeneous, single-phased materials with tunable isotropization temperatures dictated by the $\mathbf{M}_1/\mathbf{M}_2$ ratio of the copolymers.

Introduction

Glassy side-chain liquid crystalline polymers (SC-LCPs) have been widely studied in the past¹ as a materials approach that uniquely combines the mechanical and thermal properties of polymers with the optical properties of small-molecule liquid crystals, with numerous possible applications.² It is over the past two decades that researchers have focused more on cross-linked SC-LCPs because of the interesting thermomechanical properties they exhibit as liquid crystalline elastomers (LCEs).³ Indeed, *side-chain* nematic LCEs have been shown to display spontaneously large strain-reversible actuation and soft elasticity when exposed to specific stimuli.^{4,5} Here, a thermally stimulated actuation behavior, shrinking on heating through a clearing transition and expanding on cooling through the same, has been explained by a coupling between liquid crystalline order and rubber elasticity resulting from the underlying cross-linked structure.⁶ Yet higher actuator performance has been anticipated⁷ and recently demonstrated for *main-chain* liquid crystalline elastomers (MC-LCEs) because of an enhanced coupling between their intrinsically high, yet labile, orientational order and network strain compared to their side-chain analogues.⁸ Challenges exist, however, for main-chain liquid crystalline polymers, particularly regarding their synthesis and subsequent processing into elastomers. More specifically, main-chain LCPs (MC-LCPs) usually ex-

hibit comparatively high transition temperatures relative to room temperature, so that, to date, they have not received adequate attention. In addition, aside from some studies examining network architecture variation, only limited attention has been given to other important synthetic variables when dealing with cross-linked structures, particularly the influence of mesophase type, nematic, cholesteric, or various smectic on the resulting thermomechanical behavior.

A general lack of knowledge regarding the structure–property relationships in these materials, coupled with their high potential to yield improved thermomechanical properties (i.e., soft actuation), has led us to study new MC-LCPs for eventual incorporation into elastomeric structures by chemical or physical cross-linking. We are particularly interested in understanding the influence of mesogen structure and flexible spacer length as well as the various polymer architectures, homopolymers, blends, and copolymers, on liquid crystalline phase behavior and glass transition temperature. Such an understanding will allow tailoring of associated thermomechanical (actuation) behavior in related cross-linked structures so that their utility in strongly restrictive environments may be facilitated. An example category of such restrictive applications include biomedical devices, where both biocompatibility and low temperature activation are required. In the area of low temperature activation, we recently reported the shape-memory behavior of a new siloxane-based main-chain smectic-LC elastomer that was shown to allow the fixing of large strains for subsequent recovery on heating through the smectic-C-to-isotropic transition.⁹

Here, we report on a parallel effort in developing structure–property relationships in analogous linear

* Author to whom correspondence should be addressed. E-mail: patrick.mather@case.edu.

[†] Institute of Materials Science.

[‡] ingrid@mail.ims.uconn.edu.

[§] haihu.qin@case.edu.

^{||} Chemical Engineering Department.

polymers bearing various silicon-based spacers so as to enable property tailoring of similar structures when cross-linked into network form. We present the synthesis of two chemically similar mesogens, namely, 1,4-bis[4-(4-pentenyl)oxy]benzoyl]hydroquinone^{10,11} (**M**₁) and 2-*tert*-butyl-1,4-bis[4-(4-pentenyl)oxy]benzoyl]hydroquinone (**M**₂), that, although chemically similar, differ drastically in their phase transition temperatures. Indeed, we will show that substituting the slender mesogen, **M**₁, with a *tert*-butyl group (**M**₂) results in a 140 °C drop in the nematic–isotropic transition, thus suggesting that one could tune the thermal properties of the resulting materials upon mixing of these mesogens; i.e., “mixed-mesogen” LCPs. We thus describe the synthesis and characterization of silicon-based main-chain liquid crystalline homopolymers, blends, and copolymers using both **M**₁ and **M**₂ as mesogens. Three different silicon-based compounds were used as flexible spacers, namely, 1,4-bis(dimethylsilyl)benzene (**S**₁), 1,1,3,3,5,5-hexamethyltrisiloxane (**S**₂), and hydride-terminated poly(dimethylsiloxane) (DP = 8) (**S**₃). In addition to the effect of mesogen structure on phase behavior, we also reveal the influence of siloxane-based spacer structure on physical and thermo-optical properties of the resulting polymers.

Experimental Section

Materials and Methods. 1,1,3,3,5,5-hexamethyltrisiloxane (**S**₂) was purchased from Gelest, Inc., whereas the hydride-terminated poly(dimethylsiloxane) (**S**₃) was obtained from both Gelest, Inc. and Aldrich. 1,4-bis(dimethylsilyl)benzene (**S**₁), tetrakis(vinyl)dimethylsilyloxy)silane (**CL**), α,ω -divinyl-terminated poly(dimethylsiloxane), and the platinum-based catalyst (platinum(0)-1,3-divinyl-1,1,3,3-tetramethyldisiloxane complex in xylenes), were purchased from Aldrich with no information regarding purity given by the vendor. Hydroquinone (99%) was purchased from Aldrich and used without further purification. Anhydrous dichloromethane (99.9%) was purchased from Acros and dichloromethane (Optima) from Fisher Scientific. All other solvents were purchased from Acros. All chemicals were used without further treatment except for *tert*-butylhydroquinone (97%), which was purified by recrystallization from toluene (approximately 20 g/L) to yield white crystals. When required, analytical thin-layer chromatography (TLC) was conducted using precoated silica gel 60 F254 plates (E. Merck).

To verify the chemical structures synthesized, liquid phase ¹H NMR characterizations were performed using a Bruker AVANCE DMX500 spectrometer. The samples were prepared in either D₆-acetone or CDCl₃ at room temperature, depending on individual solubilities and chemical shifts, with tetramethylsilane (TMS) added as an internal standard.

Gel permeation chromatography (GPC, Waters Associates, 150-C Plus) with a PL-ELS 1000 evaporative light scattering detector (ELSD, Polymer Laboratories) was used to obtain molecular weights (\bar{M}_n and \bar{M}_w) relative to monodispersed polystyrene standards (472, 982, 4000, 6930, 43 000, 200 000, 400 000, and 824 000 g/mol; Polymer Standards Service-USA, Inc.), and polydispersity index (PDI = \bar{M}_w/\bar{M}_n). The samples, dissolved in THF to about 0.1 wt %, were injected at 35 °C with THF as an eluant and at a flow rate of 1.0 mL/min. A set of three columns packed with cross-linked divinylbenzene in series, thermostated at 35 °C, was used. Note that the resulting values for average molecular weights and polydispersity will not be absolute values since the chain conformation adopted by linear polystyrene (standards) is expected to be quite different from that of the liquid crystalline polymer investigated here. However, they will allow for qualitative comparison of the values obtained for the various LCP series.

Differential scanning calorimetry (DSC) experiments were performed on a TA Instruments Q100 apparatus with heating and cooling rates of 10 °C/min, unless otherwise stated, and

in a flowing N₂ atmosphere. Indium was used as a calibration standard for both the temperature and heat flow scales. Samples with weights ranging from 5 to 10 mg were encapsulated in aluminum pans for testing. Temperatures corresponding to maxima of the DSC endothermic peaks of the second heating traces were assigned as phase transition temperatures. The midpoint of the heat capacity stepwise increase was taken as the glass transition temperature, T_g , when appropriate.

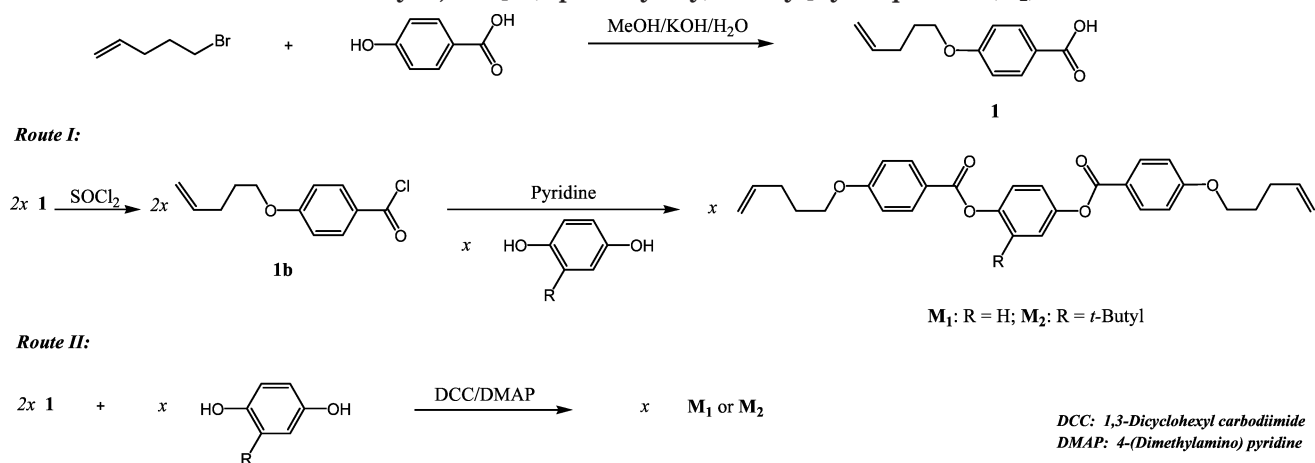
Polarizing optical microscopy (POM) studies were performed using an Olympus BX50 microscope equipped with crossed polarizers, a STC-200 hot stage from Instec Inc., and a composite color CCD camera (Panasonic GP-KR222). Images were acquired from the CCD camera at selected times and/or temperatures using a frame grabber and Linksys software (Linkam Scientific). Spatial dimensions were calibrated using a stage micrometer with 10 μ m line spacing. Unless otherwise noted, a 20x/0.4 NA achromat long working-distance objective lens (Olympus LMPlanFI) was employed. The samples used for POM analysis were sandwiched between two glass coverslips and melted on a hot stage at 150 °C, care being taken to avoid coverslip flexure that would lead to void formation, and subsequently cooled to room temperature. The temperature ramping rates were chosen to be consistent with DSC experiments for comparison purposes, and shown in this paper are micrographs obtained on second heating of the samples after an initial melting at 150 or 200 °C followed by a cooling ramp at 5 or 10 °C/min for the copolymers and blends, respectively. The hot stage was equipped with a liquid nitrogen LN2-P cooling unit from Instec, Inc. for accurate control of the sample temperature, either isothermally or during heating and cooling runs.

Wide-angle X-ray diffraction (WAXD) experiments were performed either on fibers drawn from the melt or on powdered samples using a Bruker AXS instrument with a chromium source ($\lambda = 2.291$ Å) or a Bruker AXS D8 Advance using a CuK α source ($\lambda = 1.5418$ Å). The latter was used both at room temperature and at elevated temperatures, in selected cases, with the aid of a nickel heating strip and digital temperature controller. The former was used for stretched specimens and employed a sample–detector distance of 6 cm. In both cases, the X-ray power source was operated at 40 mA and 40 kV. Data were gathered and analyzed via a general area detector diffraction system (GADDS) software version 3.317 or a Diffraction Plus software version 5.0.

Monomer Synthesis. Scheme 1 represents two different synthetic routes for the preparation of two mesogenic dienes, namely, 1,4-bis[4-(4-pentenyl)oxy]benzoyl]hydroquinone (**M**₁) and 2-*tert*-butyl-1,4-bis[4-(4-pentenyl)oxy]benzoyl]hydroquinone (**M**₂). To the best of our knowledge, **M**₂ is a new compound and so its synthesis steps are detailed below. The synthesis and purification of **M**₁ are very close to those of **M**₂ and have been previously reported by other researchers.^{10,11} Therefore, the preparation of **M**₁ is not included in this report.

Synthesis of 5-Pentenylbenzoic Acid (1). In a three-neck 500-mL round-bottom flask under stirring, 30.0 g (0.217 mol) 4-hydroxybenzoic acid were added to 135 mL of methanol, followed by the dropwise addition of 45 mL of an aqueous solution of potassium hydroxide (45 wt %). When the solution became clear, 36.6 g of 5-bromo-1-pentene (0.254 mol) was added dropwise to the solution using an addition funnel. After refluxing for 16 h, the mixture was then cooled to room temperature and poured into 500 mL of deionized water to form a transparent yellow solution. An organic phase was then extracted with 100 mL diethyl ether (alternatively, hexanes) three times. To the aqueous phase, 100 mL of a 37% hydrochloric acid solution were added, leading to the precipitation of the desired product. The precipitate, a white solid, was collected after filtration and further recrystallized from ethanol. The purity and structure were confirmed by GC-MS and ¹H NMR. The yield before recrystallization was calculated to be about 50%. ¹H NMR in D₆-acetone gave δ : 10.9 (1H, d), 7.98 (2H, d), 7.02 (2H, d), 5.88 (1H, m), 5.00 (2H, m), 4.11 (2H, t), 2.25 (2H, m), 1.90 ppm (2H, m).

Scheme 1. Schematic Representation of the Two Routes (I: Nucleophilic substitution with acid chloride, and II: Esterification under DCC catalysis) Followed for the Preparation of the Two Diene Liquid Crystalline Monomers: 1,4-bis[4-(4-Pentenyl)Benzoyl]hydroquinone (M_1), and 2-*tert*-butyl-1,4-bis[4-(4-pentenyl)Benzoyl]hydroquinone (M_2)



Synthesis of 5-Pentenylbenzoic Acid Chloride (1b**).**

In a round-bottom flask, 15.0 g (72.7 mmol) of 5-pentenylbenzoic acid, 30 mL SOCl_2 , and several drops of DMF (as catalyst) were added, and the solution was refluxed for 8 h. Most of the SOCl_2 was then removed by ambient pressure distillation to yield a viscous, dark-yellow oil-like liquid. The latter was further purified by vacuum distillation. The boiling point of the final product, a pale-yellow liquid, was found to be 130 °C (0.75 mm Hg). The yield after distillation was measured to be around 52%. $^1\text{H NMR}$ in CDCl_3 gave δ : 8.06 (2H, d), 6.95 (2H, d), 5.84 (1H, m), 5.04 (2H, m), 4.06 (2H, t), 2.25 (2H, m), 1.93 ppm (2H, m).

Synthesis of M_2 by Route I. This synthetic route is similar to that reported by Shiota and Ober,¹² yet with different compounds and purification procedures. First, 7.90 g (35.2 mol) of **1b** was added to a 250-mL round-bottom flask and cooled to 0 °C with the aid of an ice bath. Then, a solution of *tert*-butylhydroquinone in pyridine (0.75 M) was added dropwise

until stoichiometric equivalence had been reached. The resulting mixture was stirred for 4 h at $T = 0$ °C and, subsequently, for 8 h at room temperature. The reaction solution remained homogeneous (clear) throughout the reaction. After removal of solvent by evaporation, the raw product (a waxlike brown solid) was collected and purified by column chromatography using silica gel as the stationary phase and a mixture of ethyl acetate and hexanes (1:7 v/v) as eluent. $^1\text{H NMR}$ in D_6 -acetone gave δ : 8.16 (4H, m), 7.33 (1H, s), 7.22 (2H, t), 7.14 (4H, m), 5.95 (2H, m), 5.04 (4H, m), 4.16 (4H, t), 2.28 (4H, m), 1.93 (4H, m), 1.39 (9H, s) ppm (see Figure 1).

Synthesis of M_2 by route II. To a 250 mL Erlenmeyer flask, 8.0 g (0.039 mol) of **1**, 8.0 g (0.039 mol) of 1,3-dicyclohexyl carbodiimide (DCC) (note: **1** and DCC have the same molecular weight), 3.23 g of prepurified *tert*-butylhydroquinone (0.0194 mol), 0.430 g of 4-(dimethylamino)pyridine (DMAP) (3.52 mmol), and 80 mL of anhydrous dichloromethane were added. The solution quickly became milky as the reactions

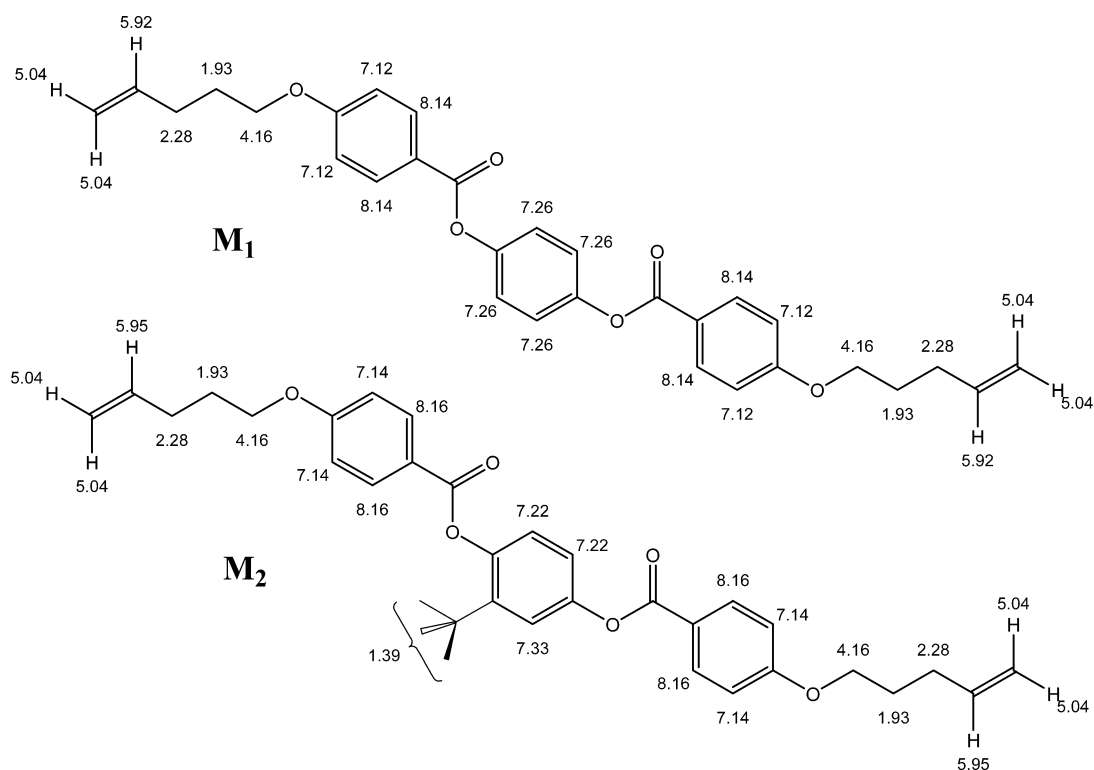


Figure 1. Schematic representation of the chemical structures of M_1 (top) and M_2 (bottom) along with the chemical shifts of each hydrogen as measured by $^1\text{H NMR}$.

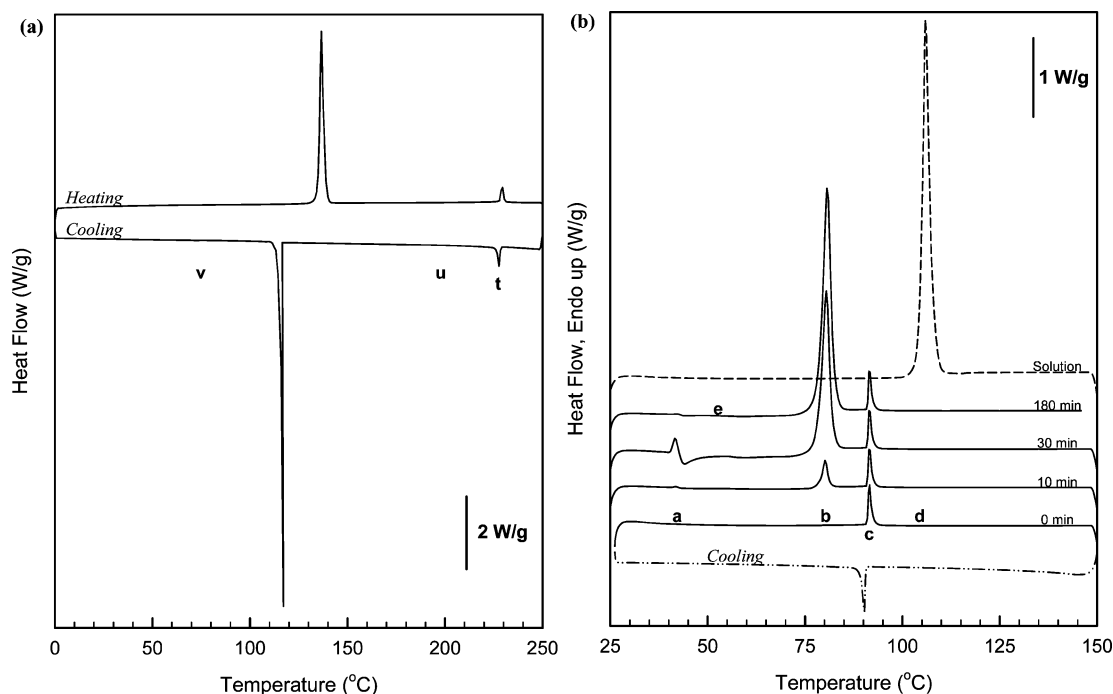


Figure 2. DSC traces at 10 °C/min of: (a) 1,4-bis[4-(4-pentenyl-oxyl)benzoyl]hydroquinone (M_1), and (b) 2-*tert*-butyl-1,4-bis[4-(4-pentenyl-oxyl)benzoyl]hydroquinone (M_2). For each trace shown, thermal history has been erased through an initial melting at 250 °C for M_1 and 150 °C for M_2 (except for the sample crystallized from solution) followed by a cooling at 10 °C/min down to 0 °C. (a) On heating, M_1 crystals melt into a nematic phase at 136.6 °C ($\Delta H = 78.24$ J/g), which clears at 229.5 °C ($\Delta H = 5.50$ J/g). (b) On heating, M_2 crystals formed from solution melt into an isotropic phase at 105.9 °C ($\Delta H = 73.08$ J/g), whereas M_2 crystals formed from the melt, after annealing at 0 °C for 3 h (indicated times), melt into a nematic phase at 80.6 °C ($\Delta H = 50.97$ J/g), which further clears at 91.4 °C ($\Delta H = 3.55$ J/g). The cooling trace is identical for all runs and only displays the isotropic-to-nematic transition.

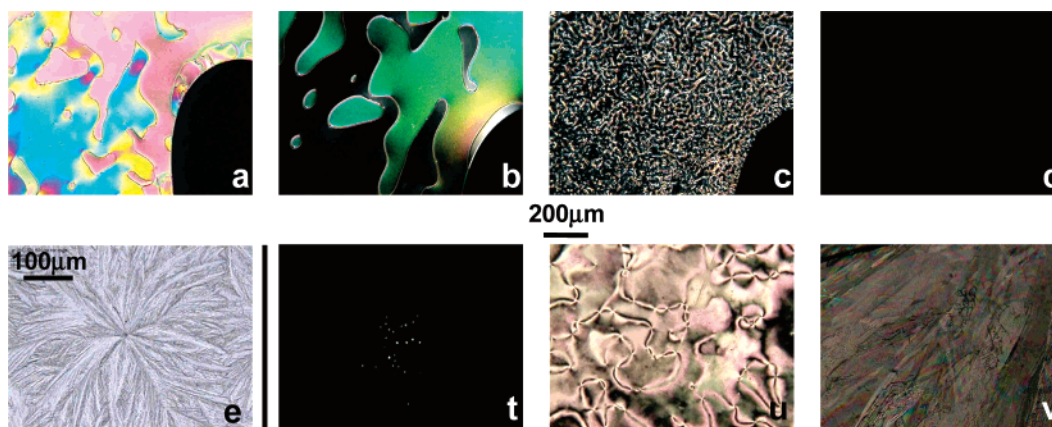


Figure 3. POM images under crossed polarizers of the mesophases exhibited by M_1 and M_2 under varying temperature. The letters refer to the mesophases exhibited by M_1 and M_2 as depicted in Figure 2. M_2 not annealed on heating at (a) 56.8, (b) 83.4, (c) 86.0, and (d) 91.2 °C. (e) M_2 crystals formed from the melt after annealing for 3 h at room temperature. M_1 on cooling from (t) the isotropic phase at 240 °C to (u) the nematic phase at 237.1 °C to (v) the crystalline phase at 71 °C. The 200 μm scale bar refers to every image except (e).

Results and Discussion

Mesogen Characterization. The phase behavior of both M_1 and M_2 were probed using differential scanning calorimetry (DSC), the results of which are presented in Figure 2. Upon heating at 10 °C/min, M_1 displays (Figure 2a) transitions in the form of sharp endothermic peaks at 136.6 (crystal–nematic) and 229.5 °C (nematic–isotropic), the first featuring a latent heat approximately 10-fold the second. By comparison, M_2 appears to have a more complex behavior (Figure 2b), with differences depending on sample history; precipitated from solution or cooled from the molten state. In the former case, M_2 exhibits a single endotherm at

105.9 °C (crystal–isotropic), while, in the latter case, two transitions are evidenced by two endotherms occurring at about 80.6 (crystal–nematic) and 91.4 °C (nematic–isotropic), the crystal–nematic transition taking time at room temperature to develop (Figure 2b, 180 min). A combination of DSC analysis with polarizing optical microscopy (POM) (see Figure 3) and wide-angle X-ray diffraction (WAXD) studies (not shown here) permitted the determination of the nature of these transitions as indicated. In particular, Figure 3 shows selected POM images acquired at temperatures indicated by letters that correspond to particular regions on DSC traces of Figure 2. POM images “a” through “d”

reveal a nematic threaded texture (a, b) for M_2 that clears through a narrow nematic–isotropic biphasic (c) to an isotropic liquid (d). If crystallized, however, M_2 exhibits featherlike crystals that grow radially with significant branching (e). Cooling M_1 from the isotropic phase (t) leads to a nematic Schlieren texture (u), populated primarily by wedge-type disclination lines, and subsequently to a dark (scattering) crystalline phase (v).

WAXD patterns for both M_1 and M_2 were consistent with POM and DSC findings, while allowing clear identification of low-temperature phases. In particular, M_1 exhibited a multitude of crystalline reflections at $T = 30$ °C (supplementary data), consistent only with a crystalline phase.^{15–16} Heating to $T = 145$ °C, a condition between the endotherms of Figure 1a and for which a nematic Schlieren texture is evident in Figure 2, only an amorphous halo in WAXD was observed (d -spacing = 4.86 Å), allowing conclusion of a nematic phase with local order (birefringent domains with domain size $1 < a < 50$ μm) but macroscopic disorder (WAXD halo). Like M_1 , M_2 is crystalline at room temperature, as evidenced by numerous diffraction peaks in WAXD observations. Interestingly, the crystal structure of M_2 depends on preparation conditions, with clear differences in peak positions and d -spacings for solution-crystallized material and melt-crystallized material.

Thus, we have observed that, at low temperatures, M_1 exists in a crystalline form, which melts to a nematic phase at 136.6 °C and further clears to an isotropic phase at 229.5 °C. These observations stand in contrast with the conclusions made by Kossmehl et al. regarding their characterization of the same compound.¹⁰ In their report, the authors described a smectic-to-nematic transition followed by a nematic-to-isotropic transition at similar transition temperatures, largely on the basis of DSC analysis. Although we are unable to explain the difference in our results, the ability of our material to crystallize to such a large extent (Figure 2a) suggests very high purity that may not have been achieved in the other study. In the case of M_2 , we observed that crystallization is more complex and seems to yield two different crystalline forms whether nucleated in solution or upon cooling from the melt. While crystals formed from solution directly melt to an isotropic phase at a comparatively high $T_m (= T_{ki}) = 105.9$ °C, crystals that form on cooling subsequently melt to a nematic phase at a significantly lower $T_{kn} = 80.6$ °C, i.e., one-time monotropism, and clear to an isotropic phase at $T_{ni} = 91.4$ °C. Moreover, crystallization of M_2 following a first melting is greatly retarded, such that cooling to $T = 0$ °C at 10 °C/min does not result in any crystallinity (Figure 2b, cooling). Instead, annealing at 0 °C for 30 min or longer is required to complete crystallization.

The similar chemical structures of M_1 and M_2 , combined with their contrasting phase behavior, suggested the promise of blending their polymeric derivatives to allow preparation of new thermotropic liquid crystalline materials with both low and tunable transition temperatures as dictated by prescribed composition. Thus, in the following sections, we present the synthesis of main-chain siloxane-based liquid crystalline polymers, blends, and copolymers, each incorporating varying amounts of M_1 and M_2 and using different silicon-based flexible spacers. We further discuss their phase behavior and structures in light of their potential use in network form for thermally stimulated actuation.

Table 1. Summary of the Homopolymers' Physical, Thermal, and Phase Characteristics

samples	\bar{M}_w (kDa)	PDI	transition temperatures (°C)
PM₁S₁	22.2	1.73	SmC + Cr 152.2, N 158.1 I
PM₂S₁	60.9	1.59	Ig 57.4 I
PM₁S₂	66.5	1.91	Sm 135.5, SmC 169.8 I
PM₂S₂	163.2	2.25	LCg 18.5, LC^a 38.9 I

^a After annealing for 8 h at 10 °C. Phases are indicated as follows: **Cr**: crystalline phase. **SmC**: smectic-C. **Sm**: undefined higher-order smectic phase. **N**: nematic. **LC**: undefined liquid crystalline phase. **I**: isotropic. **LCg**, **Ig**: liquid crystalline or isotropic glass. Polymers bearing spacers **S_i** and mesogens **M_i** are defined as **PM_iS_i**, where **M₁** is 1,4-bis[4-(4-pentenyl)oxy]benzoyl hydroquinone, **M₂** 2-tert-butyl-1,4-bis[4-(4-pentenyl)oxy]benzoyl hydroquinone, **S₁** 1,4-bis(dimethylsilyl) benzene, and **S₂** 1,1,3,3,5,5-hexamethyltrisiloxane.

Polymers and Blends Characterization. Scheme 2 gives a representation of the synthetic route for the homopolymerization of M_1 and M_2 with two different silicon-based flexible spacers, namely, 1,4-bis(dimethylsilyl)benzene (**S₁**) and 1,1,3,3,5,5-dimethyltrisiloxane (**S₂**), along with the blending procedure. Although the synthesis of M_1 has been described by other groups, preparation of the *tert*-butyl-substituted counterpart has not been reported before, and only one report on its incorporation in polymers has appeared from our group.¹⁷ Here, we show the results obtained upon polymerization, via conventional hydrosilylation reaction, of this new mesogenic unit with different siloxane and silane spacers, **PM₂S₁** and **PM₂S₂**, as well as their behavior when blended with their M_1 polymeric homologues, **PM₁S₁** and **PM₁S₂**. The physical characteristics of the homopolymers, on the basis of DSC, POM, and WAXD analyses, are summarized in Table 1. In all cases, relatively high molecular weights were achieved, with \bar{M}_w ranging from 22 to 163 kDa, and yields spanning from 45 to 92%. As expected from previous studies,^{13,18–20} the glass transition, T_g , of the M_2 -based homopolymers decreased considerably upon polymerization with longer and/or more flexible spacers ranging from about 56 °C, when polymerized with 1,4-bis(dimethylsilyl)benzene, to 21 °C when polymerized with 1,1,3,3,5,5-dimethyltrisiloxane, to $T_g = -17$ °C when polymerized with the longer hydride-terminated poly(dimethylsiloxane) spacer (**S₃**) (described below).

DSC thermograms for **PM₁S₁** and **PM₂S₁** are shown as the top and bottom traces of Figure 4a, respectively, while those for **PM₁S₂** and **PM₂S₂** are shown as the top and bottom traces of Figure 4b. Focusing first on the lower temperature ranges of each DSC trace, one can see the dramatic reduction in glass transition temperature observed for the two M_2 -based homopolymers (bottom traces) on increasing the spacer flexibility from that of **S₁** to **S₂**. On the basis of DSC analysis (Figure 4), POM, and WAXD (data not shown), we found that polymerizing with **S₁** gave rise to both a smectic and a nematic phase, while using **S₂** as a flexible spacer prevented the formation of a nematic phase and led to materials solely exhibiting smectic phases of different degrees of order. In particular, the top trace of Figure 4a, that of **PM₁S₁**, shows an initial endothermic transition ($T_m = 124.6$ °C) that grows upon annealing near but below this temperature, consistent with a melting transition. This melting transition is followed by a sharp transition from a smectic-C to a nematic phase and subsequent isotropization with a nematic window 28 °C in breadth. In contrast, the top trace of Figure 4b, **PM₁S₂**, features two sharp endothermic transitions, but

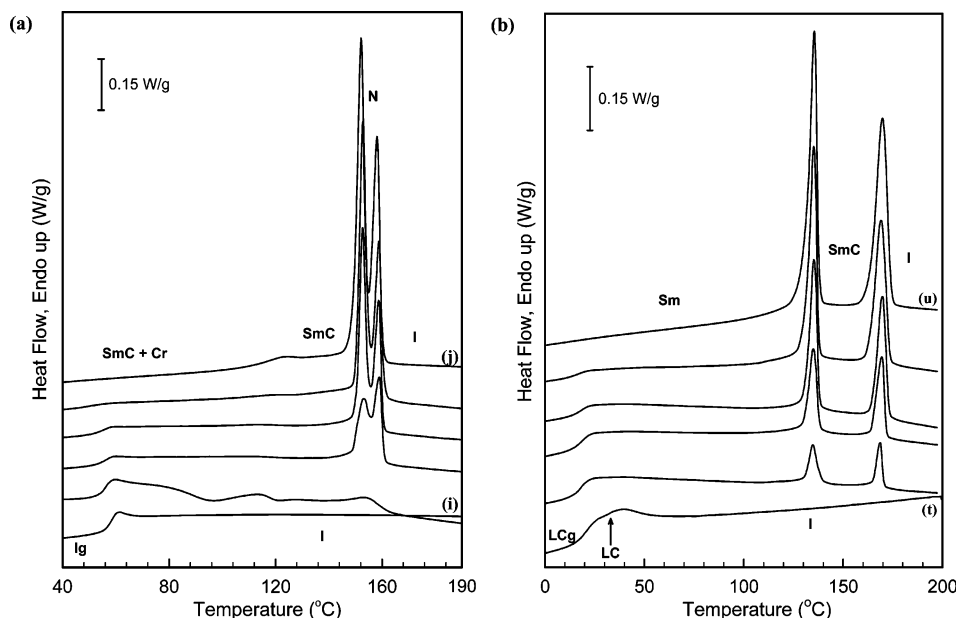


Figure 4. DSC traces of (a) various $x\text{PM}_1\text{S}_1/y\text{PM}_2\text{S}_1$ blends, and (b) various $x\text{PM}_1\text{S}_2/y\text{PM}_2\text{S}_2$, on second heating at $10\text{ }^\circ\text{C}/\text{min}$. From bottom to top, the curves indicate increasing content of the M_1 -based homopolymer in the blends via increments of 20 mol %, so that (i), (j), (t), and (u) correspond to pure PM_2S_1 , PM_1S_1 , PM_2S_2 , and PM_1S_2 , respectively. The trace (t) of PM_2S_2 corresponds to an annealed sample at room temperature so as to clearly demonstrate the existence of $\Delta H_{\text{LC-I}}$. (Sm: undefined smectic phase of high order, smectic phase. SmC: smectic-C. N: nematic. I: isotropic; LCg: liquid crystalline glass or isotropic glass. Cr: crystalline phase).

this time more widely separated and featuring a low-temperature smectic \rightarrow smectic-C \rightarrow isotropic phase sequence confirmed with hot-stage WAXD and POM. An attempt to describe the low-temperature smectic phase is given below. Hence, the S_2 spacer has a greater propensity toward smectic phase formation than the S_1 spacer.

While we suspect the nature of the low-temperature smectic phase of PM_1S_2 to be of crystalline order because of the sharp reflection at $4.14\text{ }\text{\AA}$ as well as the shallower reflections at lower angles (6.30 , 6.70 , and $7.56\text{ }\text{\AA}$) obtained from X-ray measurements (Supporting Information), we were not able to specify its structure with certainty. We speculate that it is a G -like phase²¹ (a type of smectic), whose POM texture and X-ray diffraction pattern are consistent with the ones obtained in this study; however, we presently classify it as “smectic (Sm)” until its nature can be defined with more confidence. The d -spacing values characteristic of the smectic layering of PM_1S_1 and PM_1S_2 were determined to be 24.3 and $26.8\text{ }\text{\AA}$, respectively (Supporting Information), with the associated reflection being nonisotropic with multiple off-meridian peaks for fiber samples. In the case of PM_1S_1 , the WAXD fiber pattern is consistent with a chevron microstructure wherein mesogens are oriented in the fiber direction and further assembled into inclined smectic layers. The smectic d -spacing value ($24.3\text{ }\text{\AA}$) is in good agreement with the calculated value of $26.2\text{ }\text{\AA}$ obtained using the extended conformation of the repeat unit constituting each smectic layer ($33.6\text{ }\text{\AA}$) tilted at an angle of 38.8° to the smectic normal, in accordance with the measured angle between this normal and the stretching direction (director).

The microstructure of PM_1S_2 , while similar to PM_1S_1 , is more complex, revealing 10 low-angle (smectic-like) reflections (Supporting Information), suggesting a complex chevron pattern that involves multiple inclination angles (0 , 17.6 , and 49.7°) of the smectic layers, but with constant layer spacing of $26.9\text{ }\text{\AA}$. Thus, each smectic

layer, regardless of inclination, contains mesogens tilted at an angle of 40.3° with respect to the smectic normal, using a fully extended repeat unit length computed to be $35.6\text{ }\text{\AA}$.

Inspection of the lower DSC traces of Figure 4a and b reveals that both homopolymers PM_2S_1 and PM_2S_2 (those solely incorporating M_2 as mesogen) exhibit a single thermal transition being a well-defined glass transition temperature at 57.4 and $19.1\text{ }^\circ\text{C}$, respectively. Hot-stage POM of the same samples at temperatures above these T_g values (data not shown) indicated complete absence of birefringence, confirming the isotropic nature of the materials above T_g . However, on annealing below T_g , PM_2S_1 exhibits an additional endotherm slightly higher than T_g indicative of a liquid crystalline-to-isotropic transition. Apparently, in homopolymers formed with these particular spacers, S_1 and S_2 , the pendant t -butyl group is bulky enough to suppress or delay alignment in a nematic phase or ordering into smectic layers, respectively. This behavior is in stark contrast with thermotropic LCPs with the same mesogen, but bearing substantially shorter, all-hydrocarbon spacers of eight (both saturated²² and unsaturated²³) and ten²⁴ methylene units. For these polymers with shorter spacers, crystallization is still suppressed, but a nematic phase is observed with nematic–isotropic transition much higher than those of PM_2S_1 and PM_2S_2 , being in all cases higher than $170\text{ }^\circ\text{C}$. Thus, we conclude that the spacer itself plays a leading role in determining phase ordering, at least when paired with a mesogen featuring a bulky pendant group like the t -butyl group used in this study.

Upon blending PM_1S_1 with PM_2S_1 (1,4-bis(dimethylsilyl)benzene spacer) and PM_1S_2 with PM_2S_2 (tri-siloxane spacer), we expected to observe miscibility given their similarity in chemical structure, but instead we found the pairs to be immiscible. Focusing on the intermediate composition traces in Figure 4a and b reveals simple additivity of the homopolymer traces (top

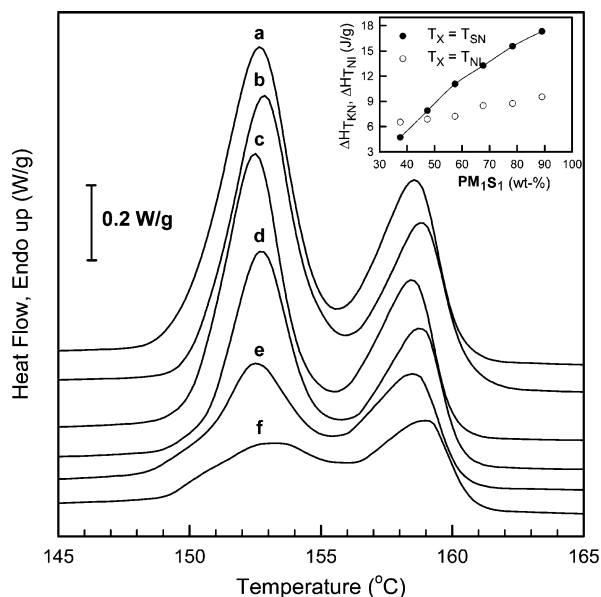


Figure 5. Close inspection of the last two endothermic transitions ($T_{SN} \approx 152$ °C and $T_{NI} \approx 159$ °C) of several $\text{PM}_1\text{S}_1/\text{PM}_2\text{S}_1$ blends: (a) 90/10, (b) 80/20, (c) 70/30, (d) 60/40, (e) 50/50, (f) 40/60. Inset: the relative variation of each endothermic enthalpy as a function of the blend composition. This shows the propensity of PM_1S_1 -rich blends to form a smectic phase, in contrast to PM_2S_1 -rich blends, while all compositions in this range maintain a similar nematic phase.

and bottom traces) with weighting of the feature sizes in proportion to the amount of that component. For example, the 60 PM_1S_1 /40 PM_2S_1 blend shows a T_g essentially unmodified from the PM_2S_1 homopolymer (54.5 and 57.4 °C, respectively), while the combined endothermic latent heats for the smectic–nematic and nematic–isotropic transitions are 55.5% of pure PM_1S_1 . Similar findings are observed for other blends in this series with the ratio $\Delta H_{\text{blend}}/\Delta H_{\text{PM}_1\text{S}_1}$, exhibiting direct proportionality to the weight percentage PM_1S_1 in the blend. On closer inspection, we observe in Figure 5 that the nematic–isotropic transition enthalpy drops less quickly with increasing PM_2S_1 in the blend than does the smectic–nematic enthalpy, indicating that the amorphous component is more disruptive to smectic ordering than to nematic alignment for the case of the S_1 spacer.

Similar behavior prevails in the case of $\text{PM}_1\text{S}_2/\text{PM}_2\text{S}_2$ blends, DSC results of which are shown as the intermediate traces of Figure 4b. In these cases, the lower PM_2S_2 -derived T_g remains virtually unchanged at 19 °C for all of the blends, and the two endothermic transitions (undetermined smectic \rightarrow smectic-C and smectic-C \rightarrow isotropic) decrease in enthalpy in nearly direct proportion to the amount of amorphous PM_2S_2 added (Figure 6). However, in contrast to the $\text{PM}_1\text{S}_1/\text{PM}_2\text{S}_1$ blends, we found that the enthalpy of the higher temperature transition (smectic-C \rightarrow isotropic) decreases with increasing PM_2S_2 content with a similar sensitivity to that of the lower-temperature smectic \rightarrow smectic-C transition (Figure 6). We reason that because of both the similarity of the liquid crystalline phases and the fact that PM_2S_2 itself exhibits liquid crystallinity (in contrast to PM_2S_1), the change in blend composition does not affect the persistence of each smectic phase relative to the other. In light of these findings, it seems that the difference in phase behavior between M_1 - and M_2 -bearing LCPs dominates over chemical similarity in

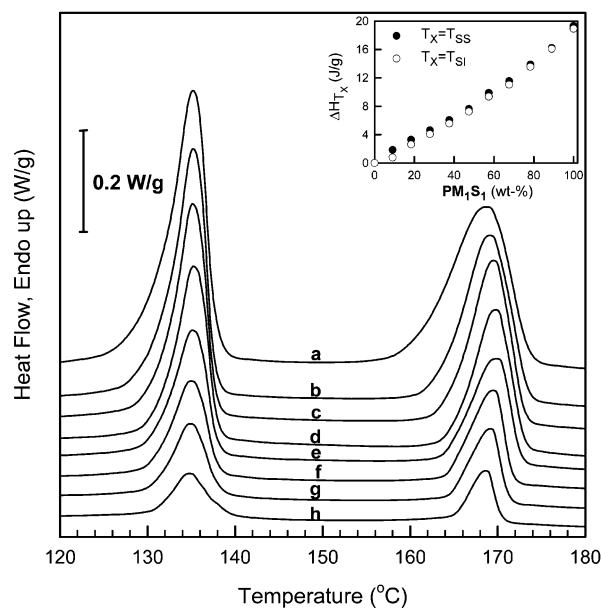


Figure 6. Close inspection of the last two endothermic transitions ($T_{SS} \approx 135$ °C and $T_{SI} \approx 169$ °C) of several $\text{PM}_1\text{S}_2/\text{PM}_2\text{S}_2$ blends: (a) 90/10, (b) 80/20, (c) 70/30, (d) 60/40, (e) 50/50, (f) 40/60, (g) 30/70, (h) 20/80. Inset: the relative variation of each endothermic enthalpy as a function of the blend composition. Because of the similar nature of the two smectic phases exhibited by these blends, their change in composition affects only very slightly the persistence of each phase relative to the other.

dictating the mixing behavior of these LCPs. This is in accordance with the general observation for small-molecule liquid crystals that alike phases broadly mix (often used to identify the phase of a new LC) independent of composition.

Although these new blends exhibit relatively low transition temperatures, including low glass transitions, they suffer from an inability to tailor transition temperatures with composition because of immiscibility. As our application goal is to incorporate new LCPs into networks for soft actuation with variable transition (triggering) temperature, another approach was needed. Restricting ourselves to incorporation of M_1 and M_2 mesogens, because of their desirable breadth in phase behavior, and the use of silicon-type spacers that enable low glass transition, we chose to prepare and study the behavior of analogous copolymer-based systems. Both the synthesis and properties of these new materials are therefore described in the following section.

Copolymer Characterization. As mentioned above, copolymerizing instead of blending as an approach toward mixing property contributions of mesogens M_1 and M_2 was expected to yield liquid crystalline materials of greater interest with respect to their end-use applications. In particular, this route was expected to yield homogeneous systems with transition temperatures that would vary continuously with composition. Additionally, this one-step routine (in contrast to blending) is made inherently simpler by avoiding the solvent blending step. The selection for the silicon-based spacer to be incorporated into the preparation of M_1/M_2 copolymers was based upon our observations for PM_2S_n homopolymers: increasing the flexibility from that of 1,4-bis(dimethylsilyl)benzene to 1,1,3,3,5,5-hexamethyltrisiloxane decreased T_g from 57 to 19 °C. Therefore, we postulated that increasing further the flexibility (length) of a siloxane-based spacer, to include eight

Table 2. Summary of Copolymer Properties

sample name	\bar{M}_w (kDa)	PDI	" T_g like" ($^{\circ}\text{C}$)	T_{SI} ($^{\circ}\text{C}$) ^a
P(M_1S_3)	63.5	2.16	49.3	93.0
P(90 M_1 -co-10 M_2)	56.7	1.46	47.2	72.9
P(80 M_1 -co-20 M_2)	47.9	1.53	41.8	68.4
P(70 M_1 -co-30 M_2)	43.7	1.48	30.7	60.8
P(60 M_1 -co-40 M_2)	44.5	1.55	17.7	53.9
P(50 M_1 -co-50 M_2)	58.3	1.53	7.6	49.2
P(25 M_1 -co-75 M_2)	42.8	1.51	-3.1	18.3
P(M_2S_3)	59.0	1.58	-16.7	-0.1

^a T_{SI} : smectic-to-isotropic transition temperature.

siloxane units, would lower T_g enough to yield properties at near room temperature that were independent of proximity to T_g . Thus, we selected a hydride-terminated poly(dimethylsiloxane) (DP = 8) (S_3 , Scheme 3) as the spacer used in the preparation of M_1/M_2 copolymers. The physical, optical, and thermal properties of these new copolymers are discussed below. In addition, their properties relevant to eventual use in networks as soft actuators will be briefly introduced.

Copolymers were successfully synthesized using hydrosilylation (see Scheme 3), yielding molecular weights, \bar{M}_w , ranging from 42 800 to 63 500 g/mol. The copolymers are designated as P($x'\text{M}_1$ -co- $y'\text{M}_2$), where x' and y' indicate the molar percentages incorporated in polymerizations with a stoichiometric equivalence of S_3 implied. The molecular characteristics, physical properties, and phase behavior of these new materials were studied using GPC, hot-stage POM, and DSC, the results of which are summarized in Table 2 and Figure 7. Immediately, we noticed that incorporation of S_3 as a spacer shifts the glass transition to subzero temperatures as low as $T = -17\text{ }^{\circ}\text{C}$. In Figure 7, the heating DSC trace of the mesogen-free analogue (similar to cross-linked PDMS) is also given. A clear melting transition near $-50\text{ }^{\circ}\text{C}$ is observed but no glass transition for $T > -80\text{ }^{\circ}\text{C}$. Apparently, the PDMS spacer of the copolymers is too short to permit the crystallization evident in high-molecular-weight PDMS. Moreover, it appears as if the glass transition exhibited by the copolymers arises from the mesogens themselves and not from their "soft" siloxane-based component. At higher temperatures, one can see for the copolymers that a broad endothermic transition shifts to lower temperatures continuously with increasing M_2 incorporation. This continuous adjustment in transition temperature is a clear indication of molecular-level homogeneity of mesogen distribution in the materials, in contrast to the significant heterogeneity indicated for the analogous blends.

The phase transition behavior of this series of copolymers (Figure 7) is complex, consisting of a broad ($20 < \Delta T < 50\text{ }^{\circ}\text{C}$) and complex endothermic transition but exhibiting a smectic-C phase at low temperatures, as determined by X-ray studies on oriented samples, and an isotropic phase at high temperatures. Copolymer phase transition behavior is further complicated by the presence of the glass transition that is superimposed on the clearing transition, as characterized by the significant shift in baseline that occurs near or within the transition. In addition to thermal behavior, Figure 7 also displays hot stage POM images obtained for a specific copolymer, P(70 M_1 -co-30 M_2), observed under crossed polarizers. This particular copolymer features a relatively simple (though broad) clearing transition, again superimposed on the glass transition that is seen in POM as a transition from a granular birefringent

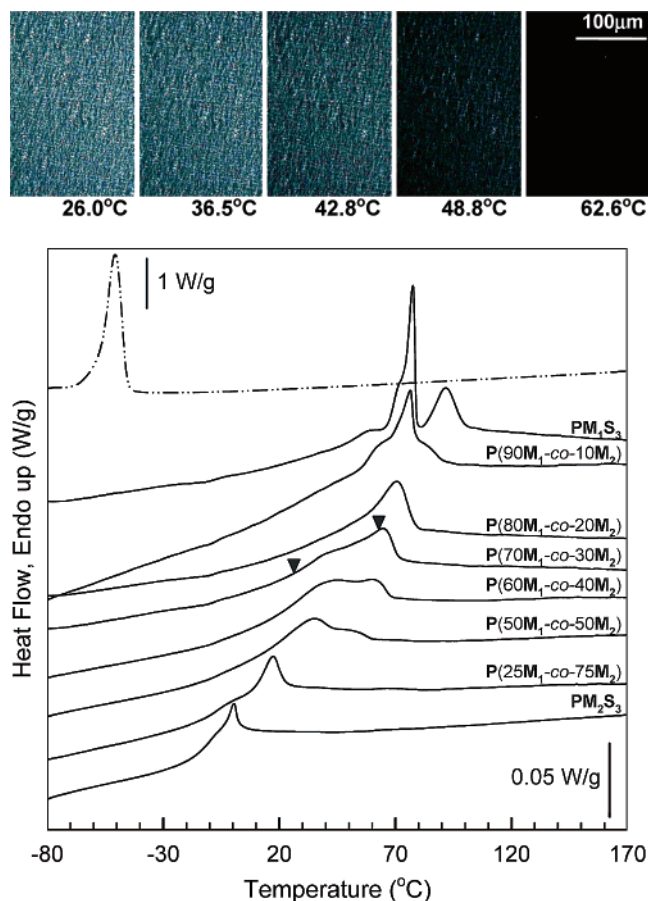


Figure 7. Thermal behavior of the siloxane-based liquid crystalline copolymers, P($x'\text{M}_1$ -co- $y'\text{M}_2$), as monitored by DSC measurements on heating at $5\text{ }^{\circ}\text{C}/\text{min}$ as a function of M_1 and M_2 . For all samples, the thermal history has been erased through an initial melting at $200\text{ }^{\circ}\text{C}$ followed by a cooling ramp at $5\text{ }^{\circ}\text{C}/\text{min}$. The POM images correspond to the temperature region demarcated by arrows for sample P(70 M_1 -co-30 M_2). The top trace corresponds to a mesogen-free analogue, revealing the absence of any glass transition in the temperature window probed for the study of the copolymers.

texture to a dark, featureless micrograph indicating optical isotropy. Physically, the material is gel-like at room temperature and liquid-like above $T_{\text{smC-I}}$, in this case, $72\text{ }^{\circ}\text{C}$. In a recent report⁹ concerning P(70 M_1 -co-30 M_2) cross-linked with a 10-mol % tetrafunctional cross-linker (tetrakis(vinyl dimethyl siloxy) silane), Rousseau et al. found that this behavior changes to a stepwise decrease in shear rubber modulus from about 10 MPa at room temperature to 100 kPa above $T = 72\text{ }^{\circ}\text{C}$.

As mentioned above, the low-temperature phase exhibited by copolymers of M_1 and M_2 with the S_3 spacer is smectic-C. Such phase order was established by gathering transmission WAXD data on samples processed into fibers drawn from the melt and cooled to room temperature. Figure 8 shows the two-dimensional (2D) WAXD pattern for P(70 M_1 -co-30 M_2) prepared in this way. In this case, we observed a pattern characteristic of a smectic-C phase, as indicated by the clear splitting of the low-angle smectic peaks into two pairs of peaks (four peaks total) separated azimuthally by roughly 45° . The second-order reflections of these smectic peaks are clearly visible (d -spacing = 16.1 \AA) and indicate a significant long-range order of the tilted smectic layers (d -spacing = 31.9 \AA). At wider angles (d -spacing = 5.7 \AA), strong and moderately sharp equato-

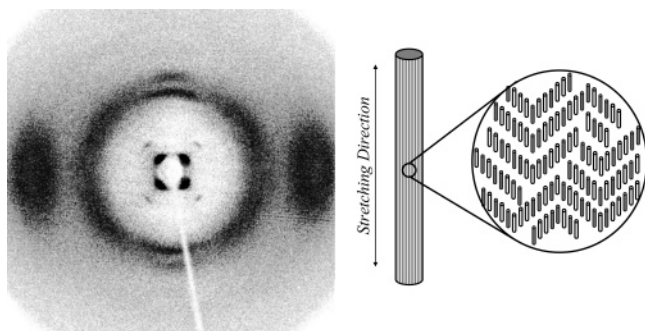


Figure 8. Two-dimensional WAXD pattern at room temperature of a $P(70M_1\text{-}co\text{-}30M_2)$ fiber drawn from the melt (drawing direction vertical). The right-hand side of the figures shows the interpreted microstructure of the underlying smectic-C phase indicated by the X-ray diffraction pattern. The two mesogens M_1 and M_2 are represented as dark and white rods, while the main-chain siloxane backbone is omitted for clarity.

rial reflections indicate strong, yet noncrystalline, intermesogen correlations within the smectic layers. At intermediate angles, an amorphous ring is superimposed with meridional layer lines corresponding to the siloxane spacers (intermediate d -spacings, 7.5 and 6.8 Å).

On the basis of these features in 2D WAXD, we envision these copolymers to exist at low temperatures in a chevronlike smectic-C layering, shown schematically in Figure 8. The measured layer spacing of 31.9 Å agrees well with the theoretical value of 34.0 Å, computed on the basis of a fully extended chain conformation arranged into tilted smectic layers adopting the measured inclination of 45° with respect to the stretching direction (see Supporting Information). The tilt angle measured for all copolymers examined in this way reside around a value of $44.9 \pm 0.7^\circ$, which is quite reasonable for such a smectic-C arrangement. Thus, the $P(xM_1\text{-}co\text{-}yM_2)$ copolymers have been shown to demonstrate broad ranges of liquid crystallinity, in some cases more than 100 °C, but also to feature relatively low isotropization temperatures that can be tuned via chemical composition to vary between 0 and 90 °C.

Such observed desirable characteristics for mixed-mesogen LCPs with siloxane-bearing spacers ($P(xM_1\text{-}co\text{-}yM_2)$) have been the goal of recent studies incorporating LC materials for actuation purposes,^{5,7,9,25} where low modulus and low triggering temperatures are required to enable certain biomedical devices.^{26–28} It is important to note that actuation phenomena in LCEs are governed mainly by: (i) their isotropization/anisotropization capabilities, which in turn dictate the conditions for actuation to occur and to what extent, and (ii) the transition temperatures, which trigger the mechanical transitions of the resulting actuators. It is the combination of these two effects that dictates the overall performances of the system. As mentioned earlier, clearing transitions for the present polymers (see Figure 7) span a wide range of temperatures. Thus, significant potential exists for these new materials to be used (in network form) as high performance soft actuators as they offer a wide range of transition temperatures easily tunable by varying the mesogen and flexible spacer composition and, therefore, a variety of end-use applications.

In addition to the experimental work done by researchers such as Finkelmann, Keller, and Ratna, which showed the immense potential of similar liquid crystal-

line materials toward spontaneously reversible actuation, preliminary studies in our group have shown that new main-chain liquid crystalline elastomers based on a similar copolymer chemistry displayed promising results in the area of shape memory,⁹ i.e., one-way actuation, and were the subject of additional studies, more to be reported. In addition, we showed that these new LC copolymers exhibit a glass transition that is superimposed on their complex clearing transition. We have reported earlier⁹ that this combination allowed for the fixing of large strains and recovery of an equilibrium shape when integrated into a shape memory design.

Conclusions

In this report, we first show the synthesis and characterization of both a new mesogen, namely, 2-*tert*-butyl-1,4-bis[4-(4-pentyloxy)benzoyl]hydroquinone, M_2 , with low transition temperatures ($T_m = 80$ °C, $T_{NI} = 91$ °C) and its already known unsubstituted homologue, namely, 1,4-bis[4-(4-pentyloxy)benzoyl]hydroquinone, M_1 , exhibiting much higher transition temperatures ($T_m = 136$ °C, $T_{NI} = 229$ °C). We believe that such difference in phase transition behavior is exclusively due to the *tert*-butyl substitution and its resulting steric hindrance on packing ability. Despite their very similar chemical structures, the drastically different phase transitions of M_1 and M_2 suggested that mixing would allow targeting of specific properties, specifically transition temperatures. Therefore, we showed the successful synthesis and preparation of new main-chain siloxane-based liquid crystalline polymers and blends incorporating M_1 and M_2 and using varying silicon-based flexible spacers. The blends obtained possessed either smectic–isotropic or smectic–nematic–isotropic mesophase sequences depending on the nature of the flexible spacer. Even though relatively low T_g and T_{NI} were achieved by blending, 20 °C and 175 °C, respectively, the immiscibility exhibited by the blends redirected us toward a copolymerization route using similar chemistry. Thus, copolymers were synthesized using hydrosilation to high molecular weights, M_w , ranging from 29 to 87 kDa, and liquid crystallinity over wide temperature windows as governed by their chemical composition. The transition temperatures of the copolymers were tuned via composition changes such that smectic–isotropic clearing ranged from 0 to 90 °C and is more or less superimposed on the glass transition that varies from about –17 to 51 °C. Such tailorability of low glass transition and isotropization temperatures renders these new materials adequate candidates for further incorporation into liquid crystalline elastomers for soft actuation devices.

Acknowledgment. P.T.M. acknowledges the support of an NSF CAREER Award, Grant CTS-00093880.

Supporting Information Available: One-dimensional (1D) X-ray diffraction patterns for M_2 ; the 1D and 2D X-ray patterns along with the azimuthal integration at low 2θ angles of both M_1 -based homopolymer fibers; a WAXD 2θ profile of a copolymer fiber drawn from the melt; azimuthal profile of WAXD low angle reflections, characteristic of the smectic-C phase, and of the large angle reflections indicative of the mesogenic ordering of the same copolymer fiber; 2D WAXD patterns for a range of M_1/M_2 copolymers. This material is available free of charge via the Internet at <http://pubs.acs.org>.

References and Notes

- (1) Pugh, C.; Kiste, A. L. *Prog. Polym. Sci.* **1997**, *22*, 601–691.
- (2) Hsu, C.-S. *Prog. Polym. Sci.* **1997**, *22*, 829–871.

- (3) Warner, M.; Terentjev, E. M. *Liquid Crystal Elastomers*; Oxford University Press: London, 2003.
- (4) Finkelmann, H.; Kock, H. J.; Rehage, G. *Makromol. Chem., Rapid Commun.* **1981**, *2*, 317–322.
- (5) Thomsen, D. L., III; Keller, P.; Naciri, J.; Pink, R.; Jeon, H.; Shenoy, D.; Ratna, B. R. *Macromolecules* **2001**, *34*, 5868–5875.
- (6) Terentjev, E. M. *J. Phys.: Condens. Matter* **1999**, *11*, R239–R257.
- (7) de Gennes, P.-G. C. R. *Acad. Sci., Ser. IIB: Mec., Phys., Astron.* **1997**, *324*, 343–348.
- (8) Donnio, B.; Wermter, H.; Finkelmann, H. *Macromolecules* **2000**, *33*, 7724–7729.
- (9) Rousseau, I. A.; Mather, P. T. *J. Am. Chem. Soc.* **2003**, *125*, 15300–15301.
- (10) Kossmehl, G.; Gerecke, B.; Harmsen, N.; Schroeder, F.; Vieth, H. M. *Mol. Cryst. Liq. Cryst. Sci. Technol., Sect. A* **1995**, *269*, 39–53.
- (11) Kossmehl, G.; Gerecke, B.; Harmsen, N.; Vieth, H. M.; Wolff, D. *Mol. Cryst. Liq. Cryst. Sci. Technol., Sect. A* **1998**, *317*, 1–21.
- (12) Shiota, A.; Ober, C. K. *J. Polym. Sci., Part A: Polym. Chem.* **1996**, *34*, 1291–1303.
- (13) Tronc, F.; Lestel, L.; Boileau, S. *Polymer* **2000**, *41*, 5039–5046.
- (14) Sellinger, A.; Laine, R. M.; Chu, V.; Viney, C. *J. Polym. Sci., Part A: Polym. Chem.* **1994**, *32*, 3069–3089.
- (15) A complete crystal structure analysis is beyond the scope of this work and is the focus of ongoing research.
- (16) Broer, D. J.; Hikmet, R. A. M.; Challa, G. *Makromol. Chem.* **1989**, *190*, 3201–3215.
- (17) Qin, H.; Chakulski, B. J.; Mather, P. T.; Constable, G. S.; Coughlin, E. B. *Polym. Prepr.* **2003**, *44*, 40–41.
- (18) Aguilera, C.; Bartulin, J.; Hisgen, B.; Ringsdorf, H. *Makromol. Chem.* **1983**, *184*, 253–262.
- (19) Sirigu, A. *Liq. Cryst. Polym.: Princ. Fundam. Prop.* **1991**, 261–313.
- (20) Diaz, F.; Tagle, L. H.; Valdebenito, N.; Aguilera, C. *Polymer* **1993**, *34*, 418–422.
- (21) Gray, G. W.; Goodby, J. W. *Smectic Liquid Crystals: Textures and Structures*; Heyden: Chichester, UK, 1984.
- (22) Lee, J.-H. Development of an Electrospinning Device for Thermotropic Liquid Crystalline Polymer (TLCP) Melts, Thesis, University of Connecticut, 2004.
- (23) Qin, Q.; Chakulski, B. J.; Rousseau, I. A.; Chen, J.; Xie, X.-Q.; Mather, P. T.; Constable, G. S.; Coughlin, E. B. *Macromolecules* **2004**, *37*, 5239.
- (24) Mather, P.; Grizzuti, N.; Heffner, G.; Ricker, M.; Rochefort, W. E.; Seitz, M.; Schmidt, H.-W.; Pearson, D. S. *Liq. Cryst.* **1994**, *17*, 811–826.
- (25) Wermter, H.; Finkelmann, H. Liquid Crystalline Elastomers as Artificial Muscles. *e-Polymers* [Online] **2001**, *13*.
- (26) Irie, M. *Shape Mem. Mater.* **1998**, 203–219.
- (27) Liu, C.; Chun, S. B.; Mather, P. T.; Zheng, L.; Haley, E. H.; Coughlin, E. B. *Macromolecules* **2002**, *35*, 9868–9874.
- (28) Lendlein, A.; Kelch, S. *Angew. Chem., Int. Ed.* **2002**, *41*, 2034–2057.

MA048327Y